Post-tensioned concrete bridge beams exposed to hydrocarbon fire

Xi-qiang Wu[1]; Ting Huang[2]; Francis Tat Kwong Au, M.ASCE[3]; Jing Li[4]

Abstract

This paper presents the experimental and numerical investigations of two types of bonded post-tensioned concrete bridge beams under hydrocarbon fire, including the box and tee beams. The factors considered included the load level and fire exposure duration. Six specimens were tested. The surface temperatures, strand temperatures and mid-span deflection of specimens were measured. Results showed that the box beam under service load could sustain fire for 184 minutes, while the tee beam could only endure for 105 minutes before collapse. The overloaded box beam could withstand fire for around 165 minutes. For exposure to fire for 90 minutes followed by cooling down to ambient temperature, the box and tee beams lost 11% and 38% of load-carrying capacity, respectively. Post-fire observation also showed severe spalling at the mid-span and support regions of the specimens. The test results were also used to validate the finite element models established for predicting the thermal and structural responses of the bridge beams under hydrocarbon fire.

[1]Ph.D. candidate, Department of Civil Engineering, The University of Hong Kong, Hong Kong, China. E-mail: wuxiqiang1988@gmail.com

[2]Ph.D., Department of Civil Engineering, The University of Hong Kong, Hong Kong, China. E-mail: ting.h0831@outlook.com

[3]Professor, Department of Civil Engineering, The University of Hong Kong, Hong Kong, China (corresponding author). E-mail: francis.au@hku.hk

[4]Associate Professor, School of Civil Engineering and Transportation, South China University of Technology, Guangzhou, China. E-mail: cvjingli@scut.edu.cn

Keywords: Bridge beam; fire tests; hydrocarbon fire curve; load level; post-tensioned concrete bridge.

Introduction

The fire-induced collapse of MacArthur Maze Bridge near Oakland, California in 2007 has reminded engineers vividly of the fire risks of bridges. It incurred a loss of nearly $ 90 million (Giuliani et al. 2012), indicating the enormous loss once a bridge fire occurs. Although fire safety is considered in building design, it is seldom required for bridges. So far only very prescriptive requirements on the fire resistance of bridges have been set out in codes such as that of American Association of State Highway and Transportation Officials (AASHTO 2002). There have been limited investigations into the damage caused by bridge fires. Most of these studies have concentrated on composite bridges (Choi et al. 2012, Gong and Agrawal 2015, Peris-Sayol et al. 2015).

While about 17% of the total fire-induced bridge failures are of concrete bridges (Wardhana and Hadipriono 2003), few studies have focused on them since concrete structures are generally considered to have better fire resistance. However, apart from the degradation of mechanical properties of materials at elevated temperatures, high thermal creep and expansion, and intense concrete spalling may also contribute to premature failure of concrete structures (Kodur 2000). The continuous heat penetration from the outer part of concrete into the rebars or tendons inside may incur further damage or even failure after fire (Giuliani et al. 2012).

Experimental work on the design of beams for buildings of high fire risk dates back to the 1960s, when rectangular post-tensioned concrete beams exposed to the ISO 834 fire curve (ISO 1999) were tested by Ashton and Bate (1960), and bonded and unbonded post-tensioned concrete tee beams exposed to the ASTM E119 standard fire curve (ASTM 2016) were tested by Gustaferro (1973). More recently, bonded prestressed continuous rectangular concrete beams under the ISO 834 standard fire were investigated by Hou et al. (2015). These results for beams in buildings under fire, however, may not apply to bridge girders because of their different cross-sections and possibly more intense fire exposure. The frequent causes of bridge fires include crashes of tanker trucks carrying highly flammable substance like gasoline (Garlock et al. 2012). Such a crash can trigger an explosion and a blaze more intense than that described by the temperature-time curves of compartment fires for building design, e.g. ISO 834 and ASTM E119 (ASTM 2016). The hydrocarbon fire curve defined in Eurocode 1 Part 1-2 (CEN 2002) featuring extremely fast increase of temperature, like that of a gasoline or diesel pool fire, is thus more suitable for bridges in such cases. Owing to the expenses of fire tests and the difficulty to monitor a real bridge fire, little experimental data is available. More recently, scale fire tests were conducted on steel-concrete composite bridge beams exposed to hydrocarbon fire by Alos-Moya et al. (2017). The responses of pretensioned concrete tee-beams strengthened by carbon fiber-reinforced polymer exposed to hydrocarbon fire were studied by Beneberu and Yazdani (2018). As the potential damage of post-tensioned concrete bridges due to hydrocarbon fire has not been studied extensively, further investigations are necessary.

This paper reports the experimental and numerical results of six scale post-tensioned concrete bridge girders exposed to hydrocarbon fire. The effects of section type, fire exposure duration and load level on their structural responses were studied.

Fire experiments

Six scale specimens labeled as S1 and F1 to F5 were fabricated, including Specimens S1 and F1 - F3 of box section, and Specimens F4 and F5 of bulb-tee section. Specimen S1 was the control specimen tested for its load-carrying capacity at ambient temperature for validation of numerical model. The other specimens were subjected to different levels of load and fire exposure as shown in Table 1. The load level is expressed as a percentage of the load-carrying capacity of the corresponding case at ambient temperature. Among the box specimens, Specimens F1 and F2 were loaded to a lower level than Specimen F3. Specimens F1 and F3 were exposed to fire until collapse at the respective load levels. Specimen F2 was heated for 90 minutes first, after which it was cooled down to the ambient temperature before further loading to failure to obtain the residual load-carrying capacity. The test schemes for Specimens F4 and F5 were similar to those of Specimens F1 and F2, respectively.

Specimen design and preparation

All specimens have a span of 4300 mm and a total length of 4600 mm (Fig. 1) to suit the furnace used. The depth of specimens is 400 mm with a span-depth ratio of about 10:1. The concrete cover to the tendon duct is 50 mm with the concrete cover to duct axis (i.e. axis distance "*ad*") of 75 mm (Fig. 1 (b)). The concrete cover to steel reinforcement is 20 mm.

Ready-mixed self-consolidating concrete with cube compressive strength of 50 MPa and mix shown in Table 2 was used for the specimens. Ordinary Portland cement, granitic coarse aggregate of size 5 - 25 mm, fine aggregate with fineness modulus of 2.5 and polycarboxylate superplasticizer were used for concrete production. The specimens were designed as fully prestressed with high-strength steel tendons initially stressed to 65% of the ultimate strength of 1860 MPa. The box specimens had 15.2 mm strands in 50 mm diameter corrugated steel ducts, while the tee specimens had 12.7 mm strands in 40 mm ducts. The effective prestressing ratios after accounting for losses according to Chinese standard GB50010-2010 (MOHURD 2010) were 49% and 51%, respectively, for the box and tee specimens. In addition, nominal longitudinal reinforcement and closed stirrups with 135° hooks at 100 mm spacing for shear resistance were provided to GB50010-2010 by 8 mm deformed bars with yield strength of 335 MPa.

Each specimen was tensioned after curing for 28 days. To avoid any damage, the strands in each specimen were tensioned alternately to 10%, 50% and 105% of the specified stress. GB50010-2010 requires that the tendons be tensioned to 105% of the specified stress and held for 2 minutes before anchoring. Strain gauges were attached to the top and bottom surfaces of the specimen at mid-span to monitor the strains during prestressing. After tensioning, grouting by cement grout with water-cement ratio of 0.45 was conducted and the pressure was maintained for 10 more seconds.

Test instrumentation

Tests were conducted using the furnace shown in Fig. 2. The facility allowed simultaneous or sequential application of loading and heating. The loading system comprised a steel reaction frame and a 500 kN hydraulic jack. The interior of furnace was 1.5 m in height, 3.0 m in width, and 4.0 m in length. All the interior surfaces of the chamber were covered with polycrystalline alumina fiber materials. Twelve natural gas burners and the same number of air inlets were alternately mounted on the chamber walls for heating. Ten thermocouples protruding from the chamber wall for 200 mm were uniformly distributed throughout the furnace chamber to monitor the gas temperature. The gas temperature inside the chamber could be adjusted by controlling the relative mass flux of fuel and air using a computer program to follow a particular fire curve. The hydrocarbon fire curve as specified in Eurocode 1 Part 1-2 (CEN 2002) was adopted to simulate the fire caused by a petroleum tanker truck. In view of the drastic increase of temperature within a very short duration, the furnace was operated at full capacity at the beginning of each test with an inflow rate of natural gas of 100 m^3/hour. This is further discussed in Section 3.1. The burnt gases were exhausted through holes at the bottom of the chamber. The internal pressure was monitored by a sensor mounted on the wall.

Each specimen was simply supported by placing it on the recesses of the opposite furnace walls, if possible, in order to be fully exposed to fire. The box specimen, however, could not fit into the recesses due to their larger width. Instead, such specimens rested on top of the furnace wall as shown in Fig. 2(b). As a result, unlike the soffit of the box itself, the soffit of the outer top flanges and the exterior surfaces of the web of the box specimen had limited fire exposure.

Strain gauges were attached to the soffit of the bottom flange of each specimen around mid-span to monitor the development of local strains prior to fire exposure. Eight linear variable differential transformers (LVDTs) were used to monitor the deformations at various locations of the specimen as shown in Fig. 1. LVDTs H1 and H2 were used to measure the horizontal displacements at the roller support and hinged support, respectively. LVDTs H3 and H4 were used to measure the incidental vertical displacements at the supports during the fire tests, which would be used for correction in calculating the net mid-span deflection. LVDTs H7 and H8 were arranged as a pair transversely and symmetrically disposed at mid-span to account for any incidental influence of torsion. The surface temperatures of the specimen and the strand temperatures at mid-span and quarter-span were measured. The thermocouples were arranged as shown in Fig. 1. In particular, the temperatures at the interior surfaces of the webs of the box specimen were also monitored. In total, 25 thermocouples were provided for each box specimen, and 22 thermocouples were provided for each tee specimen. The thermocouples for the surface temperature measurement were actually embedded in concrete with a 2 mm cover.

Testing procedure

To simulate the stress state of fully-prestressed concrete bridges under normal service load, the specimen was loaded at mid-span such that no cracking had occurred before it was exposed to fire. The loads at which the box and tee specimens would crack were estimated to be 175 kN and 72 kN, respectively, based on results from the subsequent sections on numerical modeling. Thus, the loads applied on Specimens F1 - F2 and Specimens F4 - F5 were chosen to be 160 kN and 60 kN, respectively, which were slightly below their predicted cracking loads. However, Specimen F3 was purposely loaded beyond the cracking limit up to 240 kN to induce initial cracking to simulate the response of an overloaded bridge. The ultimate load-carrying capacities of the box and tee specimens at ambient temperature were estimated to be 401 kN and 214 kN, respectively, based on the numerical models. So the applied loads corresponded to load levels of 0.28 to 0.60 as listed in Table 1.

Each specimen was loaded to the designated load level 15 minutes prior to fire exposure, and the load was maintained constant throughout the fire test. For Specimens F1, F3 and F4, the fire exposure lasted until the deflection rate exceeded the value $L^2/9000\,d$ (unit: mm/minute) given in terms of the span length L and the depth of cross section d (ISO 1999). For the tests on Specimens F2 and F5, fire exposure was terminated after 90 minutes, and air at ambient temperature was then pumped into the furnace to cool down the specimen. After cooling down to ambient temperature, these specimens were further loaded to failure to obtain the residual load-carrying capacities. The LVDTs were set to zero before the fire exposure. From then onwards, the deflections at various locations were measured throughout the test.

Numerical modeling

The modeling of the structural-fire behavior is often performed by conducting first heat transfer analysis with the surface temperatures of structure as thermal boundary conditions and then temperature-dependent nonlinear structural analysis. A sequentially coupled thermomechanical analysis was implemented by ABAQUS (SIMULA 2014). Both the thermal and structural behavior of the bridge girders during and after fire can then be analyzed.

Heat transfer analysis

By symmetry, only a quarter of each of the box and tee specimens was modeled by finite element method as shown in Figs. 3(a) and 3(b). The concrete, grout and strand were separately modeled with 8-node brick elements DC3D8. The rebars were modeled with 2-node link elements DC1D2 embedded in the concrete elements. The thermal boundaries at the exterior surfaces were defined by the specimen surface temperatures measured in the tests. The ambient temperature was assigned as the initial temperature to the interior surfaces of box specimens. The thermal properties of concrete, prestressing steel and reinforcing steel as suggested by Eurocode 2 (CEN 2004) were used. As the moisture content was not considered explicitly in the analysis, the specific heat of concrete was assigned equivalent values depending on the moisture content (CEN 2004). The moisture content of concrete in the specimens was measured as 4.0%. The densities of the concrete and steel were taken as 2400 kg/m^3 and 7800 kg/m^3, respectively.

Convection and radiation were considered at all the surfaces. The emissivity coefficient for the concrete surface was taken as 0.8 (CEN 2002). The convective heat transfer coefficient depends on the temperature. A value of 50 W/(m^2·K) was specified for the fire-exposed concrete surfaces in the heating period, while a value of 9 W/(m^2·K) was specified in the cooling period and for the unexposed surfaces (CEN 2002).

Mechanical analysis

The models used for studying the deflection behavior of the specimens were similar to those for heat transfer analysis, except that the models were built by different types of elements and prestressing was imposed. The concrete, grout and strand were modeled using solid element C3D8R. The bonding zone between the strand and grout was modeled with 3-dimensional cohesive element COH3D8. The longitudinal reinforcing bars and the stirrups were modeled with 3-dimensional truss element T3D2 embedded in the concrete element.

The pre-fire, firing, cooling and post-fire phases were modeled sequentially using ABAQUS. The external load was applied with the prescribed magnitude in the pre-fire phase and kept constant until the post-fire phase with the exception of Specimen F5 that had load reduction in the cooling phase as elaborated in the subsequent section on structural response. The temperature field results for the firing and cooling phases from the prior heat transfer analysis were used to simulate the effects of fire exposure. For specimens sustaining external load after fire exposure, further imposed displacement mimicking the imposed loading after cooling down was applied at the mid-span of specimen in the post-fire phase to determine the residual load-carrying capacity.

Material properties

The cylinder strength of concrete at ambient temperature was 50 MPa. The ultimate strength of prestressing strand and the yield strength of reinforcement at ambient temperature were 1860 MPa and 460 MPa, respectively. The material properties at elevated temperatures and after cooling were determined from those at ambient temperature as elaborated below.

The compressive and tensile mechanical properties of concrete at elevated temperatures were defined based on Eurocode 2 (CEN 2004) and the FIB code (FIB 2012), respectively. The mechanical properties of concrete after cooling were defined based on Eurocode 4 (CEN 2005). The mechanical properties of steel reinforcement at elevated temperatures and after cooling were defined based on Eurocode 2 (CEN 2004) and Eurocode 4 (CEN 2005), respectively. The mechanical properties of prestressing strand at elevated temperatures and after cooling were defined based on Eurocode 2 (CEN 2004) and Zhang et al. (2017), respectively. The bond-slip relationship of prestressing strand at elevated temperatures as proposed by Khalaf and Huang (2016) was adopted for the bonded zone. The bond properties in the cooling phase were taken to be those at the maximum temperature experienced.

Results and discussions

Load-carrying capacity at ambient temperature

The load-deflection curve for Specimen S1 tested at ambient temperature is shown in Fig. 4. The first cracking load and ultimate load-carrying capacity of the box specimen were obtained experimentally as 170 kN and 400 kN, respectively, which agreed well with the corresponding calculated values of 175 kN and 401 kN, thereby verifying the numerical models at ambient temperature. The first cracking load and ultimate load-carrying capacity of the tee specimen at ambient temperature were calculated as 72 kN and 214 kN, respectively. Unless otherwise stated, these calculated values are used as applicable.

Gas temperature

The gas temperature inside the furnace was set to follow the hydrocarbon fire curve from Eurocode 1 Part 1-2 (CEN 2002) as shown in Fig. 5, and the deviations were controlled by the lower and upper bounds according to BS EN 1363-2 (CEN 1999).

Fig. 5 showing the measured gas temperature curves obtained from the thermocouples along with the expected curve indicates that, even with the maximum inflow of natural gas, it took the furnace approximately 100 minutes to reach the hydrocarbon fire curve with a characteristic temperature of 1100 °C, which was longer than the 20 minutes specified. Nevertheless, the gas temperature curves obtained were mostly above the ISO 834 fire curve for building fire (ISO 1999) in this period. Beyond this initial period of 100 minutes, the furnace was able to follow the designated hydrocarbon fire curve. For tests on Specimens F2 and F5 which were intended for 90-minute fire exposure only, the gas temperatures were found to drop below 200 °C in 60 minutes after cooling air was pumped in and continued to decrease gradually as shown in Fig. 5.

The time equivalence method has been widely used to quantify the severity of the actual fire exposure in relation to the standard fire (Phan et al. 2010). The equal area method (Kodur et al. 2010), as one application of the time equivalence method, has been adopted in the ASTM standard (ASTM 2016) for the correction of results from test temperature curves inside a furnace. In this method, the equivalent fire duration for each test is calculated considering the deviation of the measured temperature curve from the designated hydrocarbon fire curve. The adjusted fire resistance periods shown in Table 3 can facilitate comparison on the same basis. Nevertheless, unless otherwise stated hereafter, the fire resistance period or exposure will be the experimental value without adjustment.

Thermal response

Surface temperature of specimen

The surface temperatures of specimen at the soffit of the top and bottom flanges and at the exterior surface of web are marked as top flange, bottom flange and web, respectively, and the results for the box and tee specimens are shown in Figs. 6(a) and

6(b), respectively. The temperature at the interior surface of web of the box specimen is also shown in Fig. 6(a). For those specimens heated to failure, the ultimate temperatures at the soffit of bottom flange measured 2 mm from the surface reached about 1000 °C as shown in both Figs. 6(a) and 6(b), which were slightly lower than the surrounding gas temperatures of around 1100 °C. In general, the surface temperature of the specimen was the highest at the bottom flange and the lowest at the top flange for the heating period considered. For the tee specimen, however, the surface temperature at the soffit of the top flange was initially slightly higher than that at the web for approximately 40 minutes. A vortex might have formed near the surface of the web thereby weakening the heat transfer, due to the geometric shape.

Strand temperature

The strand temperatures as shown in Figs. 7(a) and 7(b) for the box and tee specimens, respectively, were normally lower than the surface temperatures of specimen due to the protective effect of the concrete cover. There was invariably an apparent plateau at about 100 - 140 °C during the rise of the strand temperature. This was caused by the evaporation of moisture in the cement grout and concrete taking away heat. Liquid water was found near the anchorages about 17 minutes after the fire exposure, which coincided with the start of the temperature plateau for strands in the box specimens and the bottom strands in the tee specimens. The cement grout thus acted as an insulator at this temperature range and provided extra protection to the strand. It is also noted that the top strands in the tee specimens experienced a later occurrence of temperature plateau of longer duration during fire exposure as shown in Fig. 7(b). The strand temperatures for the box specimens and the lower and upper strand temperatures for the tee specimens were generally well predicted as shown in Fig. 7, indicating the reliability of the thermal properties and coefficients adopted in heat transfer analysis.

However, the simulation tended to underestimate the strand temperatures at the beginning and overestimate afterwards. The plateaus observed in the experimental strand temperature curves were not as obvious in the numerical curves. This can be caused by that the actual moisture content of grout exceeding the 4.0% measured for concrete. A higher value of moisture content in grout would theoretically yield a more visible plateau phase in the strand temperature curves.

As the temperature in the voids of the box specimens remained nearly unchanged after reaching around 105 °C as shown in Fig. 6(a) among various curves with an upward trend, there was most probably water accumulated inside the void coming from the concrete section during the heating process, which evaporated at around 100 °C, thereby taking away heat and stabilizing the temperature inside the void for a certain period. After the temperature plateau, the strand temperature continued increasing with fire exposure. However, the strand temperature in the tee specimen increased much faster than that in the box specimen. After fire exposure of 90 minutes, the strands in the box specimens attained about 210 °C while the bottom strands in the tee specimens attained about 430 °C. As the lower strands of the tee section were close to a few fire-exposed surfaces including the soffit and sides, they absorbed more heat compared to the strands of the box section, which were exposed to heat from one single side only. After termination of fire, the strand temperatures in Specimens F2 and F5 did not drop immediately but rather increased by about 40 °C and 170 °C, respectively, due to the penetration of residual heat.

The maximum strand temperatures attained during or after fire exposure are also summarized in Table 3. The strand temperature is generally regarded as a key parameter in the assessment of the fire resistance of prestressed concrete members. Eurocode 2 has specified a critical strand temperature of 350 °C for a load ratio of 0.7 together with a prestressing ratio of 0.60 and a safety factor of 1.15 (CEN 2004). Except for Specimen F2, the maximum strand temperatures in these scale bridge beams are found to range from 347 °C to 600 °C for the load ratio of 0.6 - 0.28 and prestressing ratio of about 0.5, indicating their limited capability in resisting hydrocarbon fire.

Structural response

Fig. 8 shows the measured strains at the soffit of bottom flange when the specimens were loaded to the designated load levels prior to fire exposure. As expected, no signs of cracking were found except for Specimen F3 that was meant to be overloaded.

The vertical displacements measured at the two ends and the horizontal displacement measured at the hinged end were very small. However, the horizontal displacement measured by LVDT H1 at the roller end was much larger, i.e. up to 40 mm, as shown in Fig. 9 where the negative value denotes inward displacement. Only the initial part of displacement is presented for Specimen F1 as the LVDT was found to be disturbed after testing.

The evolvement of the fire-induced mid-span deflection of specimens is shown in Figs. 10(a) and 10(b). For Specimens F1, F3 and F4 heated to failure, the evolvement of mid-span deflection can be divided into three distinct phases: (a) initial rapid increase, (b) gradual increase, and (c) accelerating increase. The mid-span deflections increased rapidly to 16 - 24 mm in the first 40 minutes of fire exposure, primarily because of the great thermal gradient and the resulting variations of longitudinal expansion across the section depth of the specimen, or the thermal bowing effect. After then, the increase of the deflection slowed down with only slight increment being observed, which might be related to the loss of stiffness of concrete near the fire exposed surface and the consequent rebound as in prestressed members (Gales et al. 2015). Then just prior to the failure of specimens, the deflections showed drastic increases again, possibly being dominated by further loss of prestress in tendon due to thermal creep. These phenomena of the mid-span deflection have also been observed in some previous experiments (Dwaikat and Kodur 2009, Gales et al. 2015, Hou et al. 2015, Wu et al. 2018). The simulated evolutions of mid-span deflection throughout the fire tests agree reasonably well with the corresponding experimental results as shown in Fig. 10. The discrepancy between the numerical and experimental deflection curves can be attributed to the missing plateau phase in the strand temperature curve from numerical simulation. The deflection was generally underestimated at the beginning but overestimated afterwards by the simulation, having the same trend as the prediction of strand temperature. Similarly, the predicted temperatures and deflections tended to exceed the corresponding test results in the later part of the tests. This indicates that the structural-fire behavior, including the fire resistance, of prestressed concrete structures depends largely on the strand temperature. Both the test and simulation results of Specimens F1 and F3 show longer fire resistance durations accompanied by lower strand temperatures.

The ultimate fire-induced mid-span deflections and fire resistance periods for Specimens F1, F3 and F4 are summarized in Table 3. In particular for the box specimens, the fire resistance period of Specimen F1 was 184 minutes, while Specimen F3 at a higher load level had a lower fire resistance period of 165 minutes. Compared with the box specimens, Specimen F4 of tee section only sustained a much shorter period of 105 minutes. The increase in mid-span deflection of Specimen F3 had been much higher than that of Specimen F1 since the start of fire exposure as shown in Fig. 10(a). The pre-cracking of Specimen F3 at higher load level had allowed easy heat penetration to the interior parts of concrete and strand (Ba et al. 2016), thereby accelerating the degradation of concrete and loss of prestress in tendon. Specimen F4, like Specimen F1, were also uncracked before fire exposure, but F4 exhibited a much shorter phase of gradual increase in the evolvement of mid-span deflection and failed much earlier, primarily because of the faster rising strand temperature in the tee specimen.

Fig. 10 shows that the responses of Specimens F2 and F5 before termination of fire after 90 minutes were almost identical to those of Specimens F1 and F4, respectively, but the post-fire evolvements of mid-span deflections of Specimens F2 and F5 were quite different. As the strand temperatures kept rising even when cooling air was pumped in upon turning off the gas, the mid-span deflections continued to increase. After Specimen F2 of box section had a small increase in fire-induced mid-span deflection, it gradually recovered and stabilized at 19 mm, therefore verifying that it survived the 90-minute hydrocarbon fire exposure. Although Specimen F5 of tee section was also expected to sustain the applied load after the fire, the mid-span deflection had increased so fast in the residual heat showing signs of collapse, and the applied load was gradually reduced from 60 kN to 30 kN until the fire-induced deflection stabilized at 109 mm. The post-fire maximum strand temperatures and residual fire-induced mid-span deflections of Specimens F2 and F5 are also shown in Table 3. That the strand temperature in Specimen F5 continued rising up to 600 °C after fire should have brought it close to potential failure.

Residual load-carrying capacity

After cooling down to ambient temperature, Specimens F2 and F5 were further loaded to failure to obtain the residual load-carrying capacities as shown in Table 3. When the destructive test was conducted, the specimen had already cooled down, with the surface temperature of the specimen and the strand temperature measured to be around 40 °C. The load-deflection curves for the fire-damaged Specimens F2 and F5 are shown in Fig. 4. The residual load-carrying capacities are determined as 355 kN and 117 kN, respectively. In other words, Specimen F2 of box section under a service load level of 0.4 could retain 89% of the load-carrying capacity after exposure to hydrocarbon fire for 90 minutes, while Specimen F5 of bulb-tee section under a service load level of 0.28 retained 55% or less for the same fire exposure. Fig. 4 also shows that both Specimens F2 and F5 suffered reduction in stiffness, particularly Specimen F5. The experimental and simulated load-deflection curves of Specimens F2 and F5 after fire exposure agree reasonably well with each other as shown in Fig. 4. The load-carrying capacity of Specimen F5 was overestimated by the simulation possibly because of the higher maximum temperature experienced by the prestressing strand due to concrete spalling, which was not considered in the numerical model.

Concrete spalling and cracking

Post-fire evaluation was conducted mainly focusing on the concrete spalling pattern, cracking patterns and failure mode of specimen. Spalling is often observed in fire tests, but the mechanism of concrete spalling is still not well understood. It is generally accepted that concrete spalling at elevated temperatures is caused by pore pressure due to moisture and / or thermal stress due to restrained thermal expansion (Kodur 2000). In the latter case, compressive stress in concrete will be induced by restrained thermal expansion in a direction parallel to the fire exposed surface. Upon reaching a threshold, this compressive stress is eventually released by means of breaking away of the outer layer of concrete, leading to sudden occurrence of spalling (Kodur 2000). Concrete spalling may occur earlier in those cases in which the concrete is already under high compressive stress before fire exposure. However, concrete spalling was not considered in the finite element models due to the difficulty of implementation.

Spalling was mostly found around the mid-span and support regions. The spalling phenomena in these two regions of each specimen are shown in Fig. 11. Severe spalling had occurred to Specimens F1, F4 and F5 due to either protracted fire exposure or easy heat penetration. Most of the concrete cover at the soffit and / or the bulb part of bottom flange had spalled and spalling even extended upwards over a certain height of the web. The outside of transverse reinforcement was generally exposed after concrete spalling. The spalling could even reach the longitudinal reinforcement as shown in Figs. 11(a) and 11(j). The thickest spalled layer was found to be 60 mm. Less severe spalling was generally observed for prestressed concrete beams tested under the ISO 834 and ASTM E119 fire curves (Ashton and Bate 1960, Gustaferro 1973, Hou et al. 2015).

Although being exposed to fire for limited time, Specimen F2 also suffered from some minor spalling at mid-span and more severe spalling close to the support. Specimens F1 and F2 were essentially the same in construction except that F2 was subjected to a shorter fire exposure of 90 minutes only. The concrete spalling might have started from the region near the support, as the soffit of bottom flange near the end was under higher compression because of prestressing, while that around mid-span was under lower compression or even tension under the combined effects of prestressing and external loading. That more severe spalling occurring close to the support than around mid-span was also observed on Specimen F3. Specimen F3 did not have as much spalling as Specimen F1 around mid-span over slightly shorter fire exposure, as the existing cracks on Specimen F3 under a higher service load level might have helped relieve the pore pressure and thermal stresses.

All specimens exhibited some form of flexural failure. Fig. 12 shows typical flexural cracks near mid-span position of specimens. These cracks originated from the bottom flange and extended towards the top flange. During all the tests, with the exception of Specimen F2, a loud noise probably associated with the fracture of strand was heard just before the crushing of concrete beneath the loading beam, soon after which the specimen failed. Specimen F2 also failed by crushing of concrete at the top flange beneath the loading beam, but without the loud noise.

Transverse cracks were observed on some of the surfaces unexposed to fire, e.g. the top surface of the top flange. These cracks were distributed along the beam and typically aligned with the stirrups as shown in Fig. 13. The simulation results also show that the concrete at the top flange are in tension upon cooling. The location of these cracks coincided with the stirrups since the tensile resistance of concrete at the cross section where a stirrup was located had been slightly reduced compared with that of the cross section without a stirrup.

Conclusions

Hydrocarbon fire tests were carried out on bonded post-tensioned concrete beams, including the single-cell box section and the tee section commonly adopted as bridge girders, to study the effect of load level on the fire resistance period. Based on the results, the following conclusions can be drawn:

- The fire resistance of the box beam is superior to the tee beam. For a concrete cover to duct axis of 75 mm and a load level of around 0.3 – 0.4, the box beam could sustain hydrocarbon fire for 184 minutes, which is comparable to the performance of building components under standard fire. However, the tee beam could only endure it for 105 minutes, revealing the vulnerability of this type of sections to hydrocarbon fire. The number of fire exposure surfaces surrounding the strand is therefore a key factor as the fire resistance of a prestressed structural member is heavily dependent on the strand temperature. In the tee beam, the heat can be transferred to the strand from both sides of the web as well as from the soffit of bottom flange. However, in the box beam, the heat can reach the strand mainly from one side of the web only and therefore the rise of strand temperature is much slower and lower.

- Fire exposure of the structure may result in residual deflection and loss of load-carrying capacity. After 90-minute exposure to hydrocarbon fire followed by cooling, the box beam had a residual fire-induced deflection of 19 mm and it lost 11% of load-carrying capacity. By contrast, the tee beam under the same fire exposure and cooling had a much larger residual fire-induced deflection of 109 mm and it lost 38% of load-carrying capacity. Therefore, after such a bridge is exposed to fire, proper assessment is necessary to evaluate the need for retrofitting.
- Compared to the standard fire curve for buildings, the potential hydrocarbon fire that may occur to bridges can cause more severe spalling, which can even reach the longitudinal reinforcement. More severe spalling was observed at the support region due to the high compressive stresses caused by the prestressing.
- The load level is a key parameter in relation to both the fire resistance and structural response. A higher load level normally causes not only shorter fire resistance period but also larger residual deflection. However, the cracks associated with a higher load level can relieve the pore pressure and compressive stresses caused by thermal expansion, which may alleviate the extent of spalling.
- The fire-induced collapse of the bridge beam can take place during the cooling phase after the fire is put out, as the residual heat continues to penetrate into the

structure and elevate the strand temperature. Immediate use of the bridge after the fire should be avoided.

- The numerical models validated with the test results can be used to predict the response of bonded post-tensioned concrete bridge beams of such types of section under various load levels and fire durations.

Owing to the limitations of the experimental facilities, the gas temperature inside the furnace was unable to follow the designed hydrocarbon fire curve in the initial 100 minutes. Therefore, lower fire resistance, lower post-fire residual load-carrying capacity and more severe concrete spalling could have resulted for both types of specimen if the gas temperature had followed the designed curve. In addition, the sides of box beams had limited fire exposure due to their mounting arrangement on the furnace. More severe damage would be expected if they could be lowered further into the furnace.

Supplementary materials

Figs. S1–S4 are available online in the ASCE Library (ascelibrary.org), covering the assumed material properties, and calculated degradation of load-carrying capacity and stiffness.

References

AASHTO (American Association of State Highway and Transportation Officials). (2002). *Standard Specifications for Highway Bridges*, Washington, DC.

Alos-Moya, J., Paya-Zaforteza, I., Hospitaler, A., and Rinaudo, P. (2017). "Valencia bridge fire tests: Experimental study of a composite bridge under fire." *J Constr Steel Res*, 138, 538-554.

Ashton, L. A., and Bate, S. C. C. (1960). "The fire-resistance of prestressed concrete beams." *P I Civil Eng*, 17(1), 15-38.

ASTM (American Society for Testing and Materials). (2016). "Standard test methods for fire tests of building construction and materials." *E 119-16*, West Conshohocken, PA.

Ba, G., Miao, J., Zhang, W., and Liu, C. (2016). "Influence of Cracking on Heat Propagation in Reinforced Concrete Structures." *J Struct Eng*, 10.1061/(ASCE)ST.1943-541X.0001483, 04016035.

Beneberu, E., and Yazdani, N. (2018). "Performance of CFRP-Strengthened Concrete Bridge Girders under Combined Live Load and Hydrocarbon Fire." *J Bridge Eng*, 10.1061/(ASCE)BE.1943-5592.0001244, 04018042.

CEN (European committee for standardization). (1999). "Fire resistance tests, Part 2: Alternative and additional procedures." *BS EN 1363-2*, Brussels, Belgium.

CEN (European committee for standardization). (2002). "Actions on Structures, Part 1-2." *Eurocode 1*, Brussels, Belgium.

CEN (European committee for standardization). (2004). "Design of Concrete Structures, Part 1-2." *Eurocode 2*, Brussels, Belgium.

CEN (European committee for standardization). (2005). "Design of composite steel and concrete structures, part 1-2. " *Eurocode 4*, Brussels, Belgium.

Choi, J., Haj-Ali, R., and Kim, H. S. (2012). "Integrated fire dynamic and thermomechanical modeling of a bridge under fire." *Struct Eng Mech*, 42(6), 815-829.

Dwaikat, M. B., and Kodur, V. K. R. (2009). "Response of restrained concrete beams under design fire exposure." *J Struct Eng*, 10.1061/(ASCE)ST.1943-541X.0000058, 1408-1417.

FIB (International Federation for Structural Concrete). (2012). *FIB Model Code for Concrete Structures 2010*, Lausanne, Switzerland.

Gales, J., Hartin, K., and Bisby, L. A. (2015). *Structural fire performance of contemporary post-tensioned concrete construction*, Springer.

Garlock, M. E. M., Paya-Zaforteza, I., Kodur, V. K. R., and Gu, L. (2012). "Fire hazard in bridges: review, assessment and repair strategies." *Eng Struct*, 35, 89-98.

Giuliani, L., Crosti, C., and Gentili, F. (2012). "Vulnerability of bridges to fire." *Proc., 6th Int. Conf. on Bridge Maint., Saf. and Management*, Abingdon, U.K., 8-12.

Gong, X., and Agrawal, A. K. (2015). "Numerical Simulation of Fire Damage to a Long-Span Truss Bridge." *J Bridge Eng*, 10.1061/(ASCE)BE.1943-5592.0000707, 04014109.

Gustaferro, A. H. (1973). "Fire resistance of post-tensioned structures." *J Prestressed Concr Inst*, 18(2), 38-63.

Hou, X. M., Kodur, V. K. R., and Zheng, W. Z. (2015). "Factors governing the fire response of bonded prestressed concrete continuous beams." *Mater Struct*, 48(9), 2885-2900.

ISO (International Organization for Standardization). (1999). "Fire-resistance tests-Elements of building construction, part 1." *ISO 834*, Geneva, Switzerland.

Kodur, V. K. R. (2000). "Spalling in high strength concrete exposed to fire: concerns, causes, critical parameters and cures." *Proc., Structures Congress*, Philadelphia, PA, 1-9.

Khalaf, J., and Huang, Z. H. (2016). "Analysis of the bond behaviour between prestressed strands and concrete in fire." *Constr Build Mater*, 128, 12-23.

Kodur, V. K. R., Pakala, P., and Dwaikat, M. B. (2010). "Energy based time equivalent approach for evaluating fire resistance of reinforced concrete beams." *Fire Saf J*, 45(4), 211-220.

MOHURD (Ministry of Housing and Urban-Rural Development of the People’s Republic of China). (2010). "GB50010-2010: Code for Design of Concrete Structures." Beijing, China (in Chinese).

Peris-Sayol, G., Paya-Zaforteza, I., Alos-Moya, J., and Hospitaler, A. (2015). "Analysis of the influence of geometric, modeling and environmental parameters on the fire response of steel bridges subjected to realistic fire scenarios." *Comput Struct*, 158, 333-345.

Phan, L. T., McAllister, T. P., Gross, J. L., and Hurley, M. J. (2010). "Best practice guidelines for structural fire resistance design of concrete and steel buildings." *NIST Technical Note 1681*, National Institute of Standards and Technology, Gaithersburg, MD.

SIMULA. (2014). Analysis User’s Manual. Providence, RI: Dassault Systèmes.

Wardhana, K., and Hadipriono, F. C. (2003). "Analysis of recent bridge failures in the United States." *J Perform Constr Fac*, 10.1061/(ASCE)0887-3828(2003)17:3(144), 144-150.

Wu, X. Q., Au, F. T. K., and Li, J. "Experimental investigation of post-tensioned concrete bridge beams exposed to hydrocarbon fire." *Proc., 10th Int. Conf. on Struct. in Fire*, Belfast, U.K., 505-512.

Zhang, L., Au, F. T. K., Wei, Y., and Li, J. (2017). "Mechanical properties of prestressing steel in and after fire." *Mag Concrete Res*, 69(8), 379-388.

Fig. 1. Details of specimens (unit: mm) and layout of instrumentation

Fig. 2. Furnace for fire tests: (a) overview; (b) section (unit: mm)

Fig. 3. Finite element quarter models: (a) box specimen; (b) tee specimen

Fig. 4. Load-deflection curves of Specimens S1, F2 and F5

Fig. 5. Gas temperatures inside furnace

Fig. 6. Temperatures at surface of specimen (a) F1 - F3; (b) F4 - F5

Fig. 7. Temperatures of prestressing strands for specimens: (a) F1 - F3; (b) F4 - F5

Fig. 8. Strains at soffit prior to fire test

Fig. 9. Evolvement of horizontal displacement at roller end

Fig. 10. Evolvement of fire-induced mid-span deflection during and after fire: (a) F1 - F3; (b) F4 - F5

Fig. 11. Concrete spalling of specimens: (a) F1 at mid-span; (b) F1 at support; (c) F2 at mid-span; (d) F2 at support; (e) F3 at mid-span; (f) F3 at support; (g) F4 at mid-span; (h) F4 at support; (i) F5 at mid-span; (j) F5 at support

Fig. 12. Flexural cracks near mid-span for specimens: (a) S1; (b) F1 and F3; (c) F2; (d) F4 and F5

Fig. 13. Typical thermal contraction cracks on top flange

Table 1. Key test parameters

Specimen	Type of section	Prestressing ratio		Load level	Fire exposure (minute)
		Initial	Effective		
S1	Box	65%	49%	To failure	0
F1	Box	65%	49%	0.40	Until failure
F2	Box	65%	49%	0.40	90
F3	Box	65%	49%	0.60	Until failure
F4	Tee	65%	51%	0.28	Until failure
F5	Tee	65%	51%	0.28	90

Table 2. Mix proportions of concrete

Materials	Mix proportions (kg/m^3)
Cement	393
Coarse aggregate	1115
Fine aggregate	601
Fly ash	95
Additive	6.34
Water	156

Table 3. Summary of thermal and structural responses

Specimen	Fire resistance period		Maximum exposure temperature (°C)	Maximum strand temperature during fire (°C)	Maximum mid-span deflection (mm)	Maximum post-fire strand temperature (°C)	Residual mid-span deflection (mm)	Residual load-carrying capacity (kN)
	Experimental value (minute)	Adjusted value (minute)						
F1	184	180	1176	448	96	-	-	-
F2	90	79	1017	210	22	251	19	355 (89%)
F3	165	153	1119	347	117	-	-	-
F4	105	93	1113	438	84	-	-	-
F5	90	82	1110	433	33	600	109	117 (55%)

Figure 1

Click here to access/download;Figure;Fig. 1.pdf

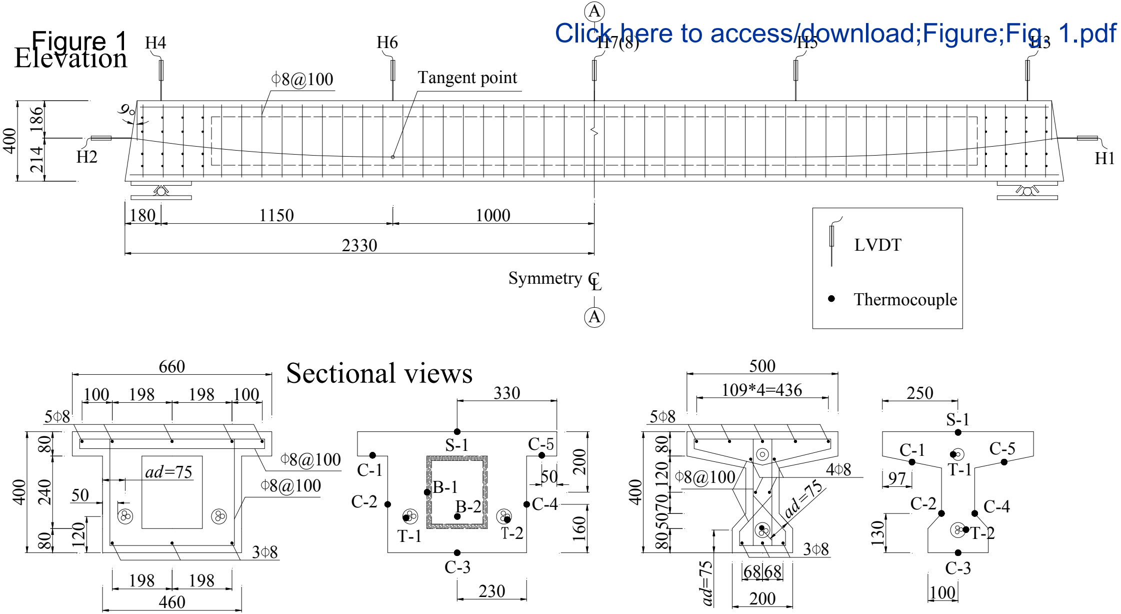

Specimens S1 and F1-F3

Thermocouples at section A of Specimens F1-F3

Specimens F4-F5

Thermocouples at section A of Specimens F4-F5

Figure 2(a)

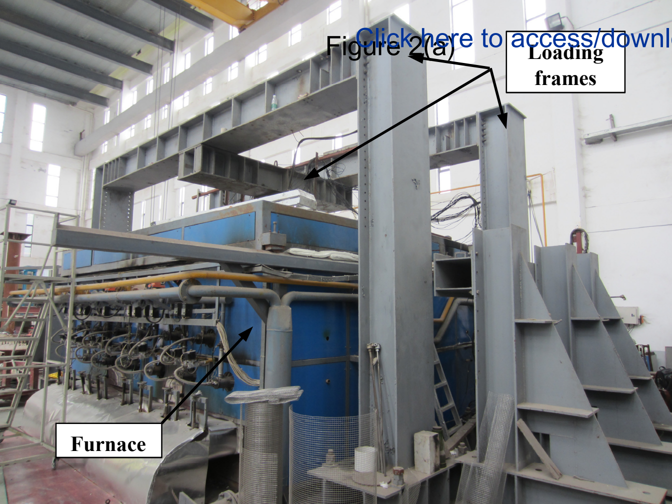

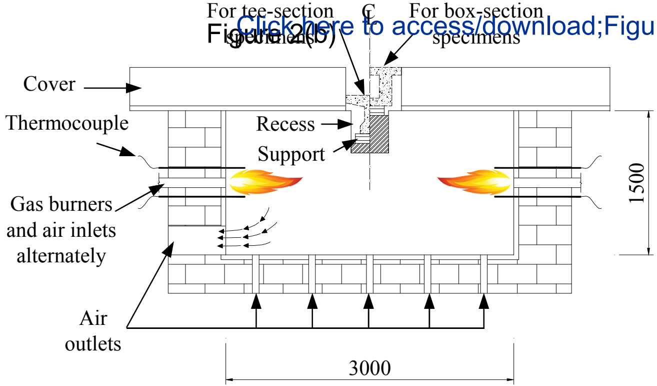
For tee-section
specimens
C
L
For box-section
specimens
Cover
Thermocouple
Recess
Support
Gas burners
and air inlets
alternately
1500
Air
outlets
3000

Figure 3(a)

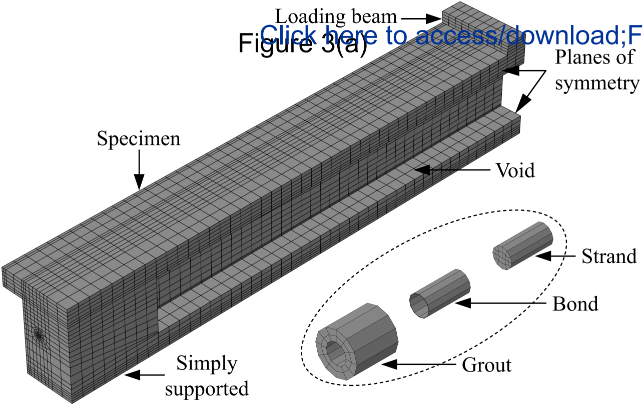
Loading beam
Planes of symmetry
Specimen
Void
Strand
Bond
Grout
Simply supported

Figure 3(b)

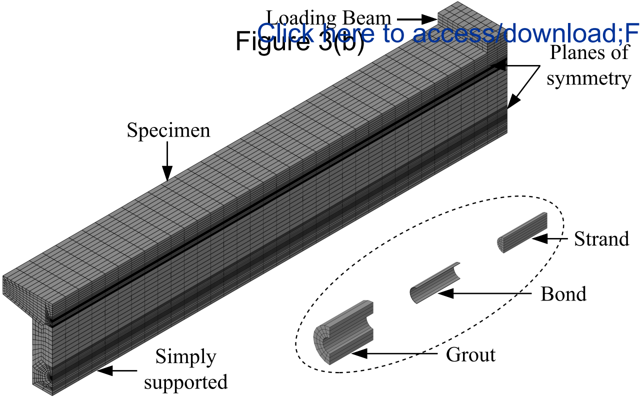
Loading Beam
Planes of
symmetry
Specimen
Strand
Bond
Grout
Simply
supported

Figure 4

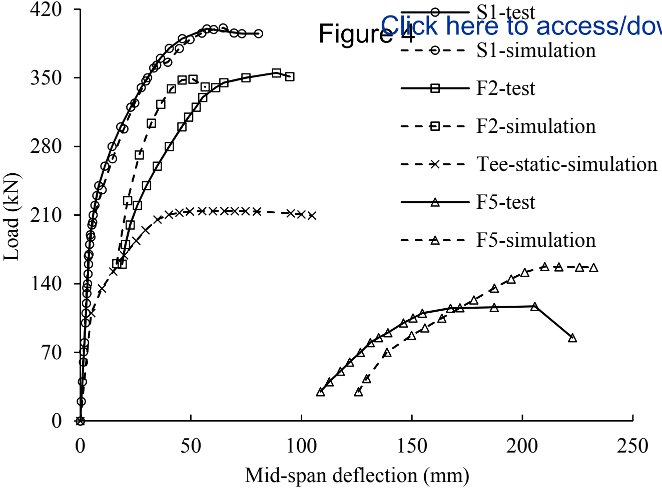

S1-test
S1-simulation
F2-test
F2-simulation
Tee-static-simulation
F5-test
F5-simulation
Load (kN)
Mid-span deflection (mm)
0
70
140
210
280
350
420
0
50
100
150
200
250

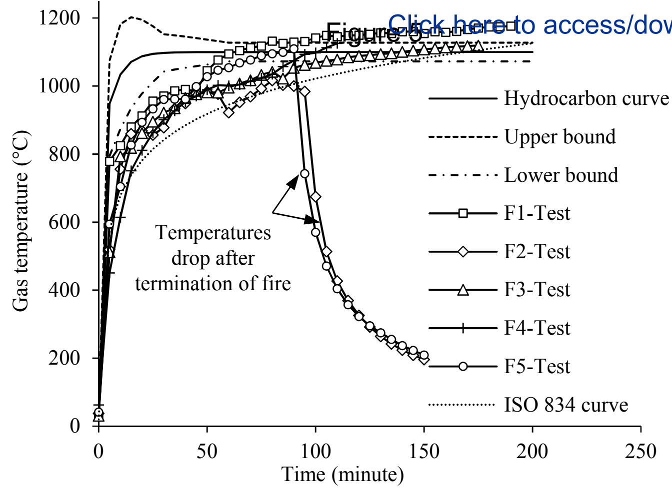

Figure 9
Click here to access/download
1200
1000
800
600
400
200
0
Gas temperature (°C)
0
50
100
150
200
250
Time (minute)
Temperatures
drop after
termination of fire
Hydrocarbon curve
Upper bound
Lower bound
F1-Test
F2-Test
F3-Test
F4-Test
F5-Test
ISO 834 curve

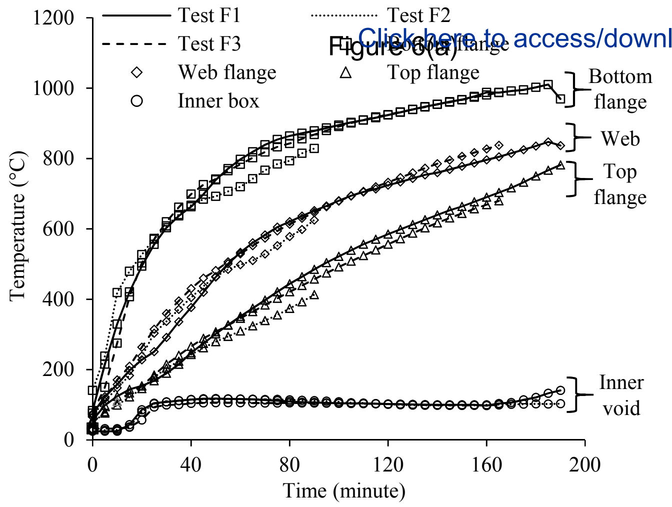

Test F1
Test F2
Test F3
flange
Web flange
Top flange
Inner box
Bottom
flange
Web
Top
flange
Inner
void
Temperature (°C)
Time (minute)
0
200
400
600
800
1000
1200
0
40
80
120
160
200

Figure 6(a)

Figure 6(b)

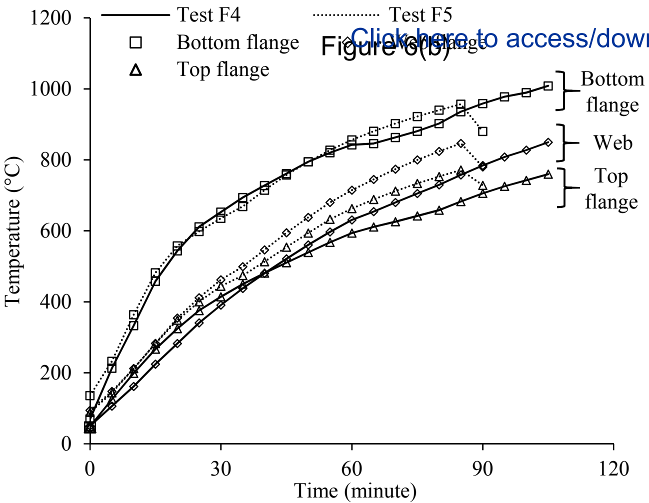
Test F4
Test F5
Bottom flange
Top flange
Web
Bottom flange
Web
Top flange
1200
1000
800
600
400
200
0
Temperature (°C)
0
30
60
90
120
Time (minute)

Figure 7(a) Click here to access/download

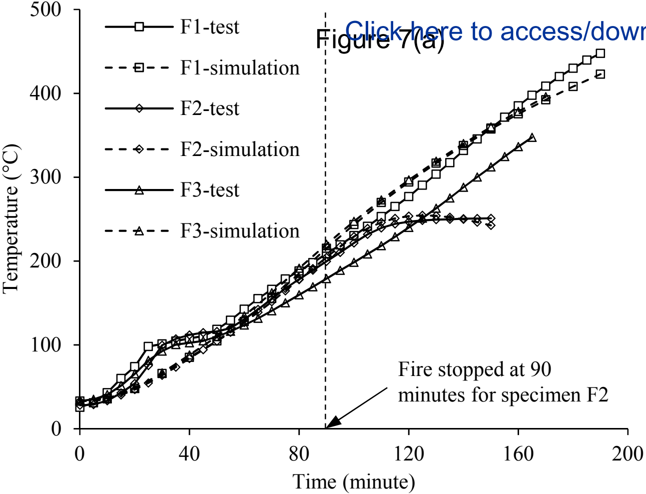

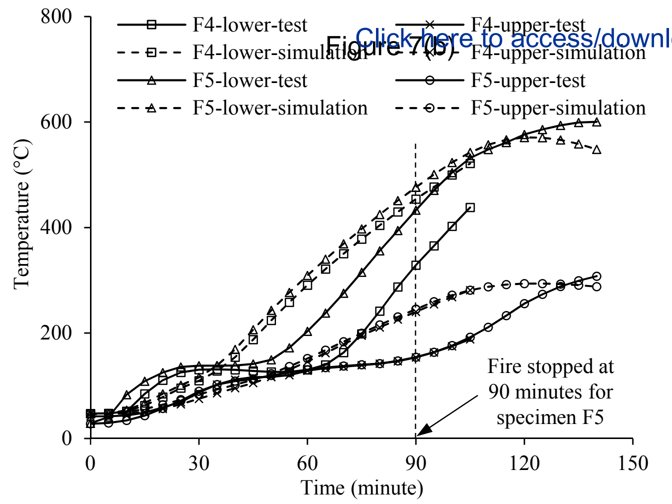

Figure 7(b)
Click here to access/download
F4-lower-test
F4-lower-simulation
F5-lower-test
F5-lower-simulation
F4-upper-test
F4-upper-simulation
F5-upper-test
F5-upper-simulation
Temperature (°C)
800
600
400
200
0
Time (minute)
0
30
60
90
120
150
Fire stopped at
90 minutes for
specimen F5

Figure 8

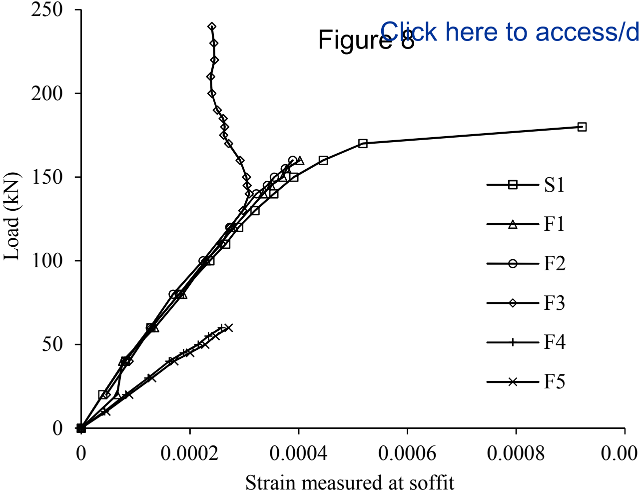
250
200
150
100
50
0
Load (kN)
0
0.0002
0.0004
0.0006
0.0008
0.001
Strain measured at soffit
S1
F1
F2
F3
F4
F5

Figure 9 [Click here to access/dow

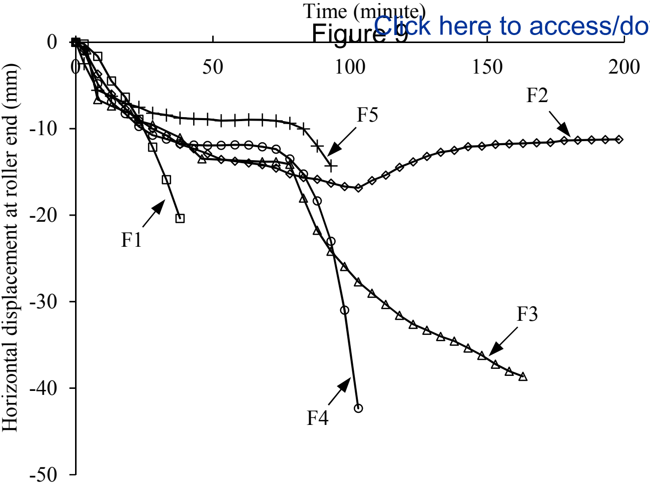

Click here to access/download
Figure 10(a)

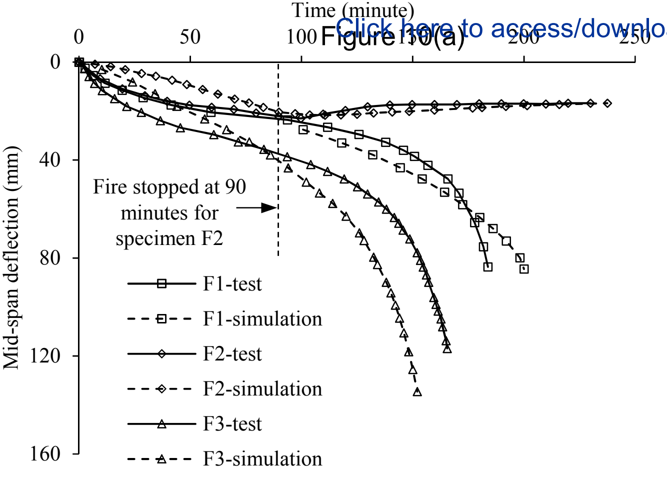

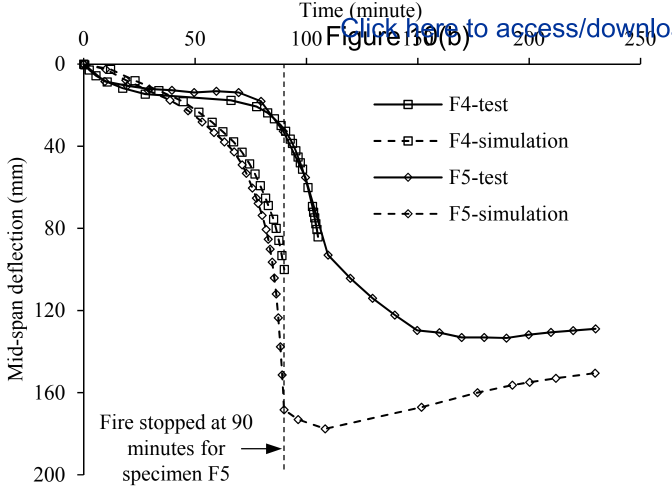

Time (minute)
0
50
100
150
200
250
0
40
80
120
160
200
Mid-span deflection (mm)
F4-test
F4-simulation
F5-test
F5-simulation
Fire stopped at 90 minutes for specimen F5

Click here to access/dow
Figure 11(a)

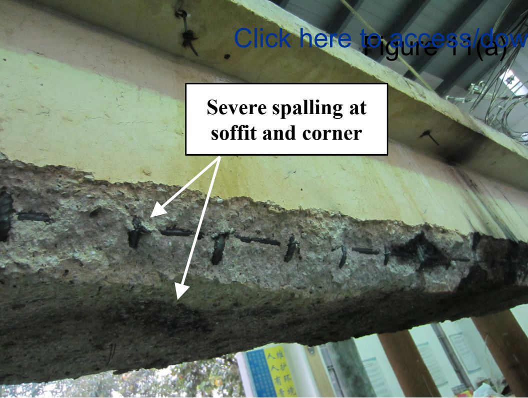

Figure 11(b)


Figure 11(c)


Severe spalling at corner
with 1.5m from support
Severe spalling at
soffit near support

Figure 11(d)

Click here to access/dow

Figure 11(e)

Figure 11(f)

Figure 11(g)

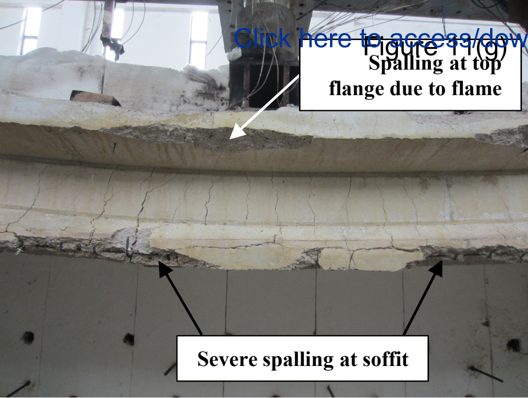
Spalling at top
flange due to flame
Severe spalling at soffit

Figure 11(h)

Figure 11(i)

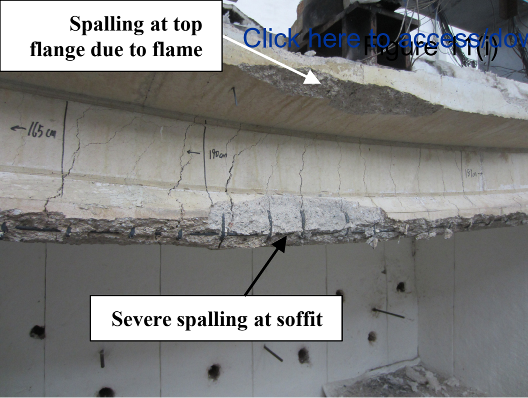
Spalling at top flange due to flame
←165 cm
190cm
Severe spalling at soffit

Figure 11(j)

Figure 12(a)

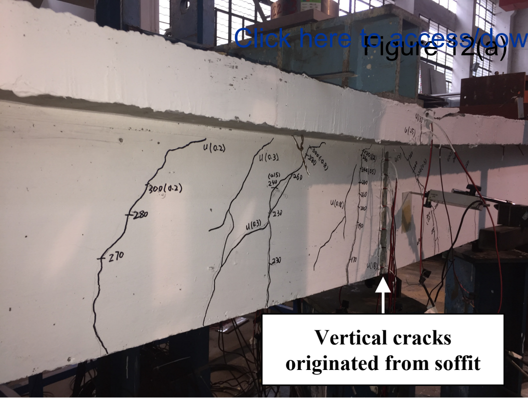
U(0.2)
300(0.2)
280
270
U(0.3)
U(0.3)
230
230
260
Vertical cracks
originated from soffit

Click here to access/dow Figure 12(b)

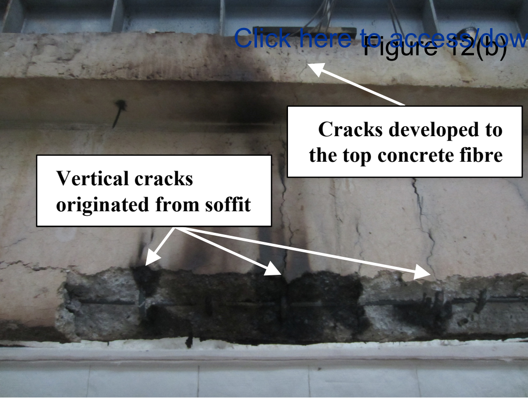

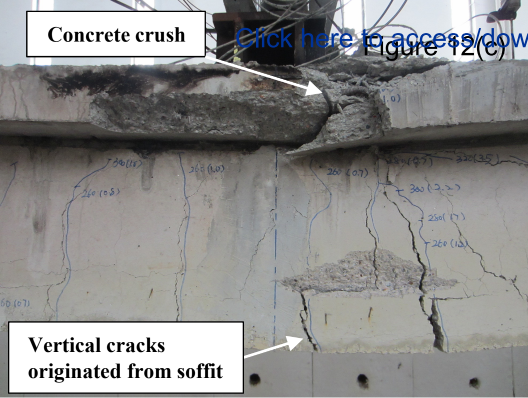
Concrete crush
Vertical cracks
originated from soffit

Figure 12(d)

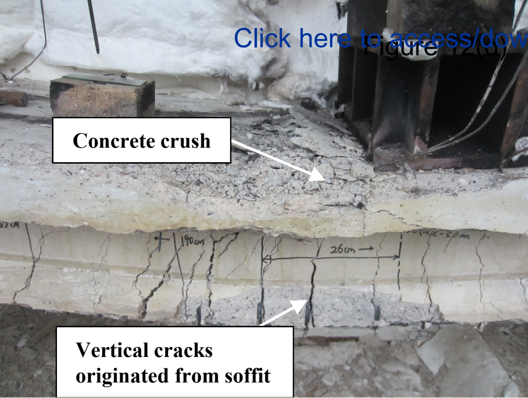
Concrete crush
190cm
26cm
Vertical cracks
originated from soffit

Figure 13

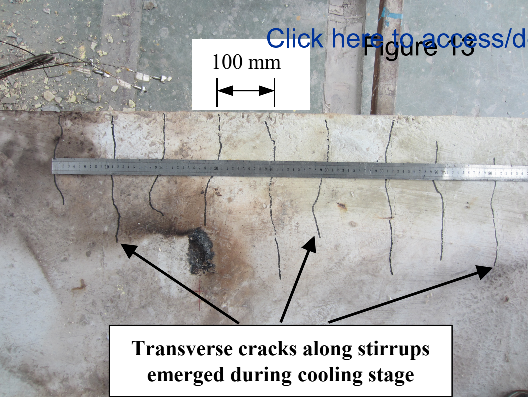
100 mm
Transverse cracks along stirrups
emerged during cooling stage